Article

Molecular Cell

Tracing Information Flow from Erk to Target Gene Induction Reveals Mechanisms of Dynamic and Combinatorial Control

Graphical Abstract

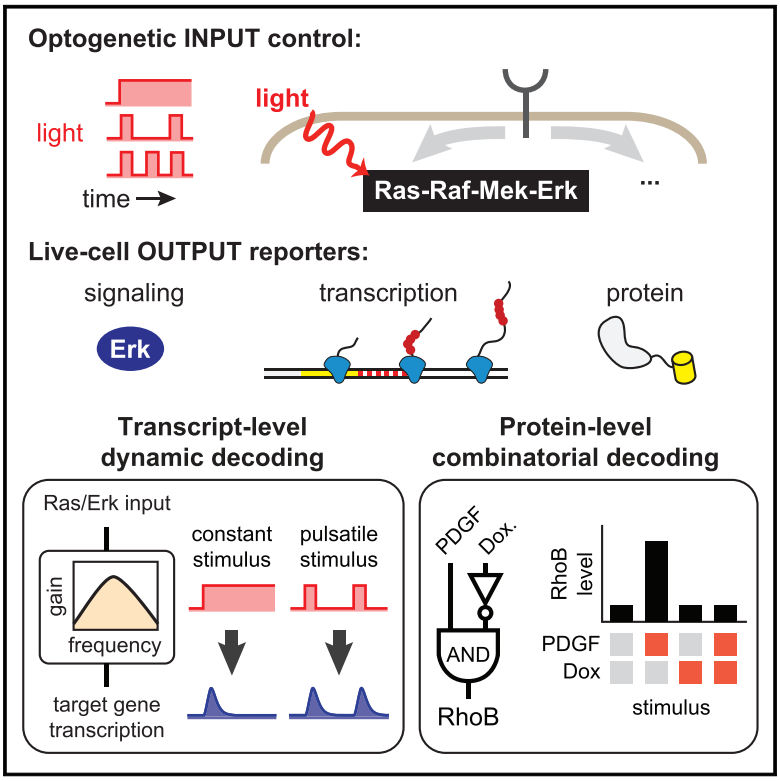

Authors

Maxwell Z. Wilson, Pavithran T. Ravindran, Wendell A. Lim, Jared E. Toettcher

Correspondence

toettcher@princeton.edu

In Brief

Signaling protein dynamics are widespread, but their biological functions are poorly understood. In this issue of *Molecular Cell*, Wilson et al. use optogenetics to control Ras signaling while visualizing target gene responses, revealing dynamic and combinatorial control of gene expression.

Highlights

- OptoSOS-IEG cells couple precise Ras control to live-cell mRNA/protein reporters
- Negative feedback on Erk converts a sustained input to a pulse of transcription
- Immediate early genes (IEGs) act as band-pass filters of dynamic input stimuli
- IEG protein accumulation is gated by combinations of upstream pathways

Wilson et al., 2017, Molecular Cell 67, 757–769
September 7, 2017
http://dx.doi.org/10.1016/j.molcel.2017.07.016

CellPress

Molecular Cell
Article

Tracing Information Flow from Erk to Target Gene Induction Reveals Mechanisms of Dynamic and Combinatorial Control

Maxwell Z. Wilson,[1] Pavithran T. Ravindran,[2] Wendell A. Lim,[3,4] and Jared E. Toettcher[1,5,*]
[1]Department of Molecular Biology, Princeton University, Princeton, NJ 08544, USA
[2]Department of Chemical and Biological Engineering, Princeton University, Princeton, NJ 08544, USA
[3]Howard Hughes Medical Institute
[4]Department of Cellular and Molecular Pharmacology, University of California, San Francisco, San Francisco, CA 94158, USA
[5]Lead Contact
*Correspondence: toettcher@princeton.edu
http://dx.doi.org/10.1016/j.molcel.2017.07.016

SUMMARY

Cell signaling networks coordinate specific patterns of protein expression in response to external cues, yet the logic by which signaling pathway activity determines the eventual abundance of target proteins is complex and poorly understood. Here, we describe an approach for simultaneously controlling the Ras/Erk pathway and monitoring a target gene's transcription and protein accumulation in single live cells. We apply our approach to dissect how Erk activity is decoded by immediate early genes (IEGs). We find that IEG transcription decodes Erk dynamics through a shared band-pass filtering circuit; repeated Erk pulses transcribe IEGs more efficiently than sustained Erk inputs. However, despite highly similar transcriptional responses, each IEG exhibits dramatically different protein-level accumulation, demonstrating a high degree of post-transcriptional regulation by combinations of multiple pathways. Our results demonstrate that the Ras/Erk pathway is decoded by both dynamic filters and logic gates to shape target gene responses in a context-specific manner.

INTRODUCTION

Cells respond to extracellular stimuli in diverse ways. They may move, grow, or adopt specific cell fates. Such responses are typically controlled at two distinct levels. Initially, signaling pathways transmit information from membrane-localized receptors to intracellular compartments within seconds to minutes. On the order of minutes to hours, intracellular pathways modulate the expression of networks of target genes to induce prolonged changes in cell state. Although both signaling pathways and their downstream target gene networks have been the subject of intensive study, major questions remain about how they are interconnected. Which signaling pathways are sufficient to induce the expression of particular sets of target genes? How do specific signaling states, defined by the combination of active pathways and their temporal dynamics, determine which target genes are induced?

Addressing these important questions has been extremely challenging because of the complex interconnections between upstream signaling and downstream target genes. Receptor-level stimulation can activate many parallel pathways with complex dynamics, making it difficult to causally relate a single pathway to a particular target gene's response. The expression of a single target gene product may also be regulated at multiple steps, from the initiation of transcription to the stabilization of protein products. Thus, an ideal approach for disentangling this complexity would have three properties. It would (1) isolate a single pathway at a time to avoid regulation by uncontrolled signaling pathway combinations, (2) exert precise control over stimulus dynamics so as to causally relate input stimuli to downstream responses, and (3) enable the experimentalist to monitor multiple nodes during the process of target gene induction to dissect regulation at each step of the central dogma.

Here, we develop an approach with exactly these properties, by coupling optogenetic stimulation with live-cell reporters of pathway activity, target gene transcription, and target protein accumulation. Optogenetic control enables the selective activation of a single pathway, greatly reducing the combinatorial complexity of the signals that are turned on by extracellular stimuli (Toettcher et al., 2013). Light can also be quickly toggled on and off, enabling the delivery of precisely defined input dynamics (Hannanta-Anan and Chow, 2016). On the reporter side, the advent of CRISPR-based genome modification has made it possible to directly tag endogenous genes with fluorescent reporters for visualizing transcription (Darzacq et al., 2009) and protein accumulation (Stewart-Ornstein and Lahav, 2016). High-resolution live-cell biosensors are also available for a growing number of intracellular signaling pathways (Regot et al., 2014). We show that these diverse technologies can be combined in a single cell to provide a full input-output view of signaling pathway transmission through the central dogma (Figure 1A).

We apply our approach to study a canonical signaling/gene expression interface: the regulation of immediate early genes

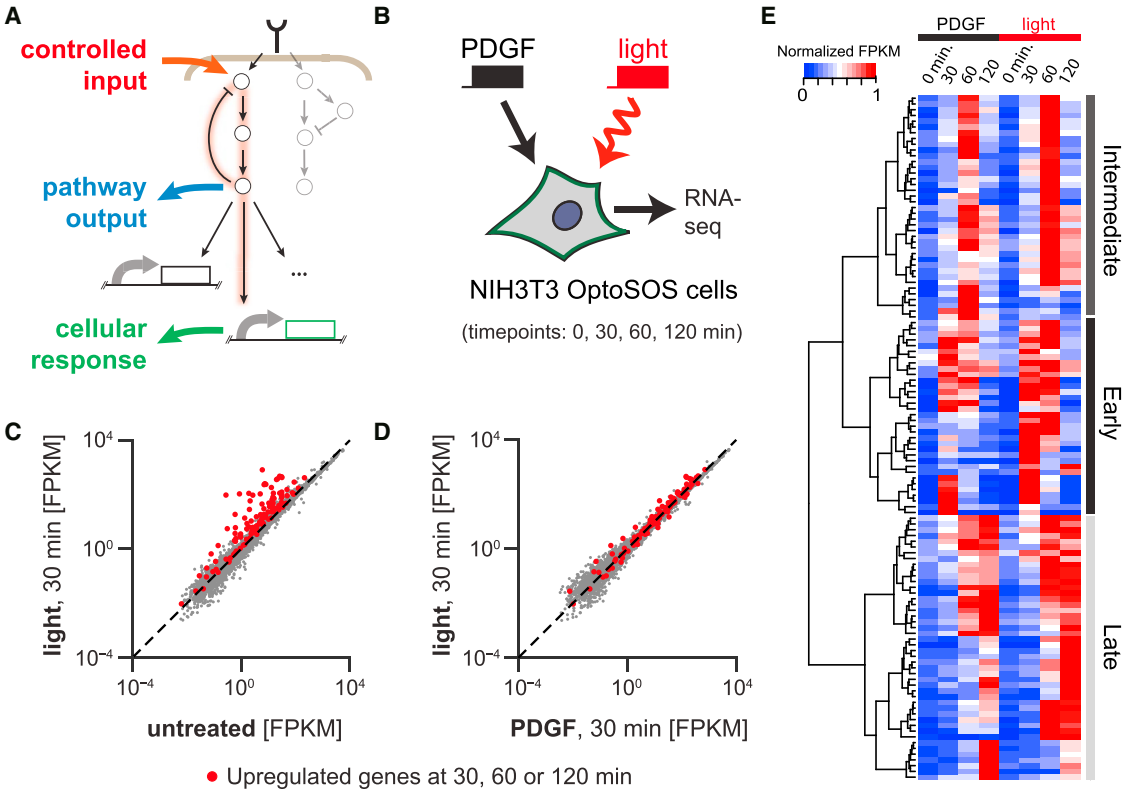

Figure 1. A Global Map of Ras-Induced Transcriptional Dynamics

(A) Schematic of an idealized system for connecting signaling dynamics to gene expression, implementing both controlled inputs and live-cell reporters at multiple nodes.

(B) To determine PDGF- and Ras-specific transcriptomes, NIH 3T3 OptoSOS cells were stimulated with PDGF or activating light and subjected to RNA-seq analysis.

(C and D) Comparison of transcript abundance between unstimulated cells and 30 min of light-activated Ras (C) or between 30 min of PDGF and 30 min of light (D). Genes that were upregulated at any time point are colored red.

(E) Transcript abundance for all upregulated genes, normalized to each gene's maximal expression condition. Genes were hierarchically clustered using Ward's method.

See also Figure S1.

(IEGs) by the mammalian Ras/Erk pathway. IEGs are among the best-characterized targets of Ras/Erk signaling and play crucial roles in learning and memory (Guzowski et al., 1999), cell proliferation, and cancer (Miller et al., 1984). They are characterized by their rapidity of response, with transcript levels peaking 1–2 hr after the addition of growth factor, and by the observation that IEG transcription does not require new protein synthesis, such that even quiescent cells are primed to induce IEGs. The expression of IEGs and other Ras-dependent genes is also thought to be subject to complex, multilayered regulation. Different growth factors can induce distinct dynamics of Erk activity, gene expression, and cell-fate outcomes (Bishop et al., 1994; Marshall, 1995), leading to the proposal that certain IEGs selectively respond to sustained, but not transient, Erk stimuli. A putative mechanism for dynamic discrimination has even been established: Erk modulates both transcription and protein stabilization for the canonical IEG Fos (Murphy et al., 2002), forming a coherent feed-forward loop that would be predicted to selectively respond to sustained inputs (Mangan and Alon, 2003).

Recent studies using live-cell pathway reporters have uncovered far more ornate Erk dynamics than the canonical transient and sustained responses. Stochastic Erk pulses, traveling waves, and long-term oscillation have been observed both in vitro and in vivo (Albeck et al., 2013; Aoki et al., 2013; Hiratsuka et al., 2015). Cellular responses that were previously thought to require sustained Erk stimulation may also be activated by specific pulse sequences, suggesting that these natural dynamics could play an important physiological role (Zwang et al., 2011). Moreover, the contribution of different pathway combinations induced by growth factors remains poorly understood (Klinghoffer et al., 2002). Together, these observations highlight the importance of revisiting questions about how time-varying Erk activity is interpreted by downstream genes with quantitative, single-cell resolution.

To address these questions, we combine precise control of Ras signaling with quantitative analysis of the dynamics of Erk localization, IEG transcription, and IEG protein accumulation in single live cells. We find that optogenetic Ras stimulation induces a highly stereotyped, transient pulse of IEG transcription,

after which IEGs remain insensitive to Ras stimulation for hours. Through a combination of mathematical modeling and experiments, we demonstrate that transcriptional adaptation implements a tunable band-pass filter on Ras/Erk dynamics. Recurrent Erk pulses can efficiently activate target genes, whereas sustained activation or infrequent Erk pulses each lead to reduced transcription. Despite sharing a stereotyped global transcriptional response, we report that IEG induction at the protein level is subject to additional, gene-specific control. Thus, different combinations of extracellular stimuli activate distinct subsets of IEGs in a manner that cannot be predicted from their transcriptional responses. Our work thus reveals that dynamic and combinatorial regulation each play crucial roles in Erk-dependent IEG induction but that these two regulatory modes act at distinct levels of the central dogma.

RESULTS

OptoSOS Stimulation Activates the Dynamic Ras Transcriptome

In prior work, we developed an optogenetic system for delivering highly precise, time-varying inputs to Ras, termed OptoSOS (Toettcher et al., 2013). This system relies on a membrane-targeted photoswitchable protein (Phy-CAAX) and a cytoplasmic Ras activator (PIF-SOScat) whose localization to the membrane can be triggered on and off by exposure to 650 and 750 nm light. We found that this system is selective for Ras/Erk and does not activate parallel growth factor signaling branches such as phosphatidylinositol 3-kinase (PI3K)/Akt, Src, or Jnk (Toettcher et al., 2013). It can also be used to deliver highly precise levels and dynamics of Ras/Erk signaling both in vitro and in vivo (Johnson et al., 2017). As a major goal of the present study is to extend the reach of our OptoSOS system to probe target gene induction, we first set out to globally assess the transcriptional response to light-activated Ras and compare it to that induced by growth factor stimulation.

We stimulated NIH 3T3 OptoSOS cells with either constant activating red light or platelet-derived growth factor (PDGF) and measured transcriptional responses by RNA sequencing (RNA-seq) (GEO: GSE100816). Total mRNA was collected after 0, 30, 60, and 120 min and used to track the dynamics of transcript abundance in both conditions (Figure 1B). Genes were defined as upregulated if they were induced at least 3-fold over unstimulated cells for at least two consecutive time points (Figures 1C and 1D, red points; Figure S1A). By these criteria, we detected 118 genes that were upregulated within 2 hr by either PDGF or light stimulation, a number of Ras-responsive genes comparable to that found in previous studies (Tullai et al., 2007).

We found that both PDGF and light induced nearly identical profiles of gene expression, with 100/118 genes induced by PDGF and 110/118 induced by light. At each time point, we found excellent agreement between the levels of gene induction in response to both stimuli (Figure 1D and S1B). This agreement also extended to response dynamics (Figure 1E), where hierarchical clustering revealed three classes of dynamic responses: an early response peaking within 30 min, an intermediate response peaking at ~1 hr, and a late response where gene expression gradually increased over the full 2-hr time course. In all three classes, we found that light and PDGF led to highly similar expression changes over time. We thus concluded that sole stimulation of the Ras/Erk pathway by light was sufficient to recapitulate at least the first 2 hr of the PDGF-induced transcriptional response.

Developing an Engineered Cell Line for Single-Cell Profiling of Ras-Dependent IEG Induction

Although RNA-seq provides a global snapshot of target gene induction, its insights are limited in some important respects. RNA-seq only reports on transcript levels, whereas signaling pathways such as Ras/Erk can influence multiple steps along the central dogma by regulating mRNA stability (Amit et al., 2007), target protein levels (Murphy et al., 2002), and even protein subcellular localization (Grimm et al., 2012). Such multi-level regulation may be important for implementing the regulatory networks that shape target gene responses (Mangan and Alon, 2003). In addition, RNA-seq relies on population-averaged measurements at a small number of time points, whereas Erk activity can vary rapidly and asynchronously across a population of cells (Albeck et al., 2013). Population-averaged measurements thus cannot be used to accurately relate signaling dynamics to target gene induction. To surmount these issues, we sought to couple our OptoSOS system to live-cell reporters of signaling pathway output (e.g., Erk activity), target gene transcription, and target protein accumulation (Figure 2A).

To do so, we took advantage of live-cell reporters that were recently developed at all three of these individual nodes. At the signaling level, we previously demonstrated that the nuclear translocation of a fluorescent Erk fusion protein faithfully tracks light stimuli delivered to the OptoSOS system (Toettcher et al., 2013). At the transcript level, the MS2/MCP system can be used to quantitatively visualize transcription from endogenous genomic loci (Garcia et al., 2013; Larson et al., 2011). In this system, multiple repeats of an RNA stem-loop (MS2 loops) are introduced into a target gene. During transcription, nascent MS2 loops are bound by a fluorescent viral coat protein (MCP-mCherry), resulting in the appearance of a bright, fluorescent spot at the site of transcription. At the protein level, we adopted the strategy of introducing a fluorescent protein fusion into the endogenous gene locus (Stewart-Ornstein and Lahav, 2016). We chose a superfolder YFP variant (msfYFP) for its fast maturation time (<10 min), enabling accurate measurement of fast changes in protein levels (Pédelacq et al., 2006). Finally, we incorporated a fluorescent histone 2B (H2B-dirFP) to label nuclei for cell segmentation (Regot et al., 2014).

We pursued a two-step approach to integrate all of these components in a single cell line. First, we generated a clonal NIH 3T3 "chassis" cell line that expresses all system components that are independent of a specific target gene (the OptoSOS system, BFP-Erk, MCP-mCherry, and H2B-dirFP) (Figure S2A). Light stimulation of the chassis cell line reversibly translocated SOScat on and off of the membrane and induced Erk phosphorylation to levels comparable with PDGF induction (Figures S2B–S2E). Second, we modified our chassis cell line to tag specific Ras-responsive target genes. We designed an msfYFP-24xMS2 reporter tag that can be integrated at the C terminus of any target

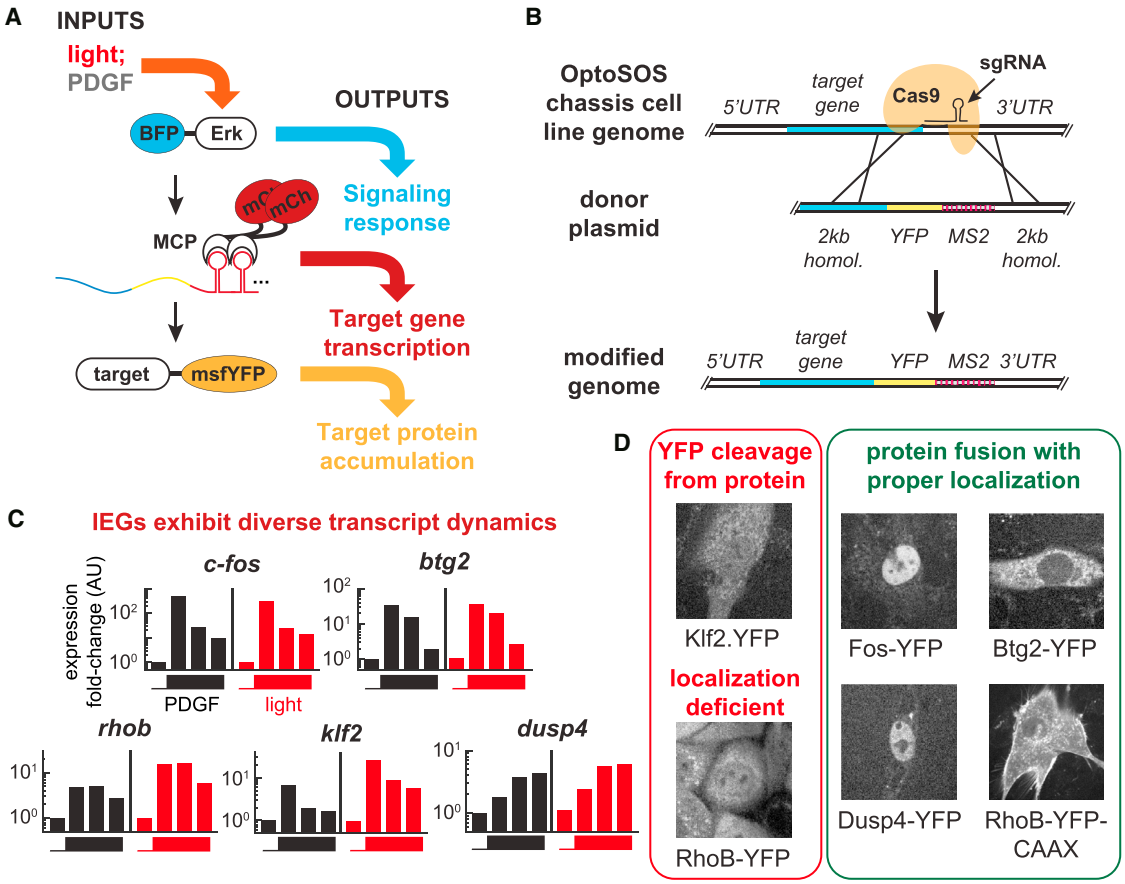

Figure 2. A System for Profiling Ras/Erk Control of IEGs in Single Live Cells

(A) Schematic overview of all-optical input-output system. Dynamic Ras stimuli can be delivered by illuminating OptoSOS cells with red/infrared light. Ras pathway activity, target gene transcription, and target protein accumulation are inferred from BFP-Erk localization, MCP-mCherry nuclear foci, and msfYFP expression, respectively.

(B) Co-transfection of Cas9 with an appropriate gRNA (guide RNA) and the msfYFP-MS2(24X) flanked by homology to the genomic cut site induces stable integration of the msfYFP-MS2 tag at an endogenous genomic locus.

(C) Fold change of expression profiles for each IEG tagged using the approach in (B).

(D) Images of msfYFP expression for each genomically tagged IEG used in this study. Red box indicates tags that are mislocalized or exhibit fluorescent protein cleavage.

See also Figure S2.

gene of interest using CRISPR-Cas9 (Figure 2B; STAR Methods). Our cassette is designed to be inserted in-frame at the C terminus of the target gene, enabling us to visualize both protein accumulation (from msfYFP fluorescence) and target mRNA production (from MCP-mCherry nuclear foci).

We used our approach to construct cell lines for five canonical IEGs: *fos*, *rhob*, *btg2*, *klf2*, and *dusp4*. These genes were chosen because they exhibited a wide range of dynamic responses by RNA-seq (Figure 2C) and are involved in diverse biological processes. After sorting for msfYFP expression, we confirmed proper integration of all five tags by genomic PCR and sequencing. Henceforth, we refer to the five resulting cell lines according to which target gene is tagged in each case (e.g., OptoSOS-Fos and OptoSOS-RhoB).

All five IEG reporter cell lines were subjected to extensive testing and validation. First, we checked whether the MS2/MCP system was able to detect stimulus-dependent transcription. Transcription could be induced by light or PDGF and was blocked by the transcription inhibitor actinomycin D or the MEK inhibitor U0126 (Figures S2F–S2I). Second, we probed lysates collected from each cell line with an anti-GFP antibody to validate that IEG-msfYFP fusion proteins were expressed at the correct molecular weight (Figure S2J). Four of five genes passed this test, but it was revealed that the msfYFP tag was cleaved from the Klf2-msfYFP fusion protein. Our Klf2.YFP cell line could thus be used to report on the rates of mRNA production and translation (by quantifying MCP-mCherry foci and YFP induction, respectively), but not total Klf2 protein levels or localization.

Third, we validated proper protein localization of each fusion protein by live-cell microscopy. This test revealed a defect in RhoB-YFP localization, which can be explained by the loss of

a functional CAAX sequence as a result of the C-terminal msfYFP fusion. We found that adding the RhoB-CAAX sequence back to the C terminus of YFP rescued RhoB's membrane localization, and comparing the levels of nuclear RhoB-YFP and membrane-localized RhoB-YFP-CAAX in individual cells demonstrated that both exhibited similar dynamics after light stimulation (Figures S2K–S2M).

Finally, to test that our tagging system did not dramatically alter mRNA or protein half-life, we measured Fos-msfYFP decay after a pulse of light-stimulated Erk (Figure S2N). Fos-msfYFP exhibited a half-life of ~40 min, consistent with published reports for the untagged Fos protein in 3T3 cells after pulsatile Erk activation (Murphy et al., 2002). Taken together, our results demonstrate the flexibility of the chassis line/CRISPR-tagging approach as a general method to track mRNA production and protein accumulation of genes of interest in single live cells.

Similar IEG Transcription Dynamics Suggest a Common Ras-Responsive Module

Our OptoSOS-IEG cell lines can be used to control Ras activity while simultaneously tracking responses at three output nodes: mitogen-activated protein kinase (MAPK) signaling output, target gene transcription, and target protein accumulation. We found that sequences of red/infrared light could be used to reversibly stimulate OptoSOS activity and gene expression, even while performing four-color fluorescent imaging at multiple z-positions to ensure that all nuclear MCP foci were captured (STAR Methods). Focusing first on the OptoSOS-RhoB and OptoSOS-Fos cell lines, we observed that pulses of activating red light drove corresponding pulses of nuclear Erk and target gene transcription, as well as the gradual accumulation of RhoB-YFP or Fos-YFP protein (Figures 3A and 3B; Movie S1).

How might information from dynamic Ras/Erk signaling be decoded into IEG accumulation? To answer this question, we imaged Erk localization, transcript production, and protein accumulation of all five IEGs (Figure 3C; Movie S2). Continuous red light stimulation led to immediate and sustained Erk accumulation in the nucleus, as expected from prior work (Toettcher et al., 2013). Light induced transcription of all five target genes with strikingly similar dynamics, reaching a transient peak of activation and then adapting back to baseline over the next hour. In contrast, we observed highly divergent responses at the level of target protein accumulation. Some gene products were strongly induced by light (RhoB and Fos), whereas for others, OptoSOS stimulation induced little to no change in msfYFP accumulation (Btg2 and Klf2). We also observed one case where nuclear-cytoplasmic shuttling, but not overall protein accumulation, responded to light-activated Ras (Dusp4). In sum, all IEGs exhibited highly similar dynamics at the transcriptional level but led to a wide variety of protein-level outcomes.

Just as in our prior transcriptomic analysis, optogenetic Ras stimulation and PDGF treatment broadly induced qualitatively similar transcript- and protein-level responses (Figure S3A). Both stimuli elicited a transient pulse of *IEG* transcription, as well as accumulation of the same IEG protein products. However, some differences were also apparent: PDGF treatment induced a pulse of nuclear Erk that decreased to an intermediate level over ~30 min, possibly due to receptor-level negative feedback (Mori et al., 1992). Consistent with the lower sustained amplitude of Erk signaling, PDGF also induced noisier transcriptional responses and reduced nuclear-cytoplasmic shuttling of Dusp4.

The light-induced transcriptional dynamics we observed were surprising for two reasons: (1) they lacked the characteristic "bursting" dynamics reported by prior studies using the MS2/MCP system (Senecal et al., 2014) and (2) they were limited in duration to the first hour of stimulation, despite continuous light stimulation and nuclear Erk accumulation. Bursts of transcription are typically explained by the probabilistic switching of a DNA locus between an "ON" state that produces mRNA and an "OFF" state with a low rate of transcription. In contrast, IEG transcription was largely deterministic; for all genes, we observed highly synchronous, sustained transcription that began 10–20 min after light stimulation and then returned to baseline over the subsequent ~1 hr (Figure 3D; Movie S2). The similarity across all five genomic loci raised the possibility that all IEGs share a single transcriptional regulatory module that initially induces a constant, high level of transcript production and then adapts over time.

We reasoned that if IEGs are regulated by a single transcriptional input module, then each gene might also exhibit a similar amplitude of transcription. Amplitude can be determined from the brightness of nuclear MCP foci, which should be proportional to the number of nascent transcripts whose MS2 stem-loops have already been transcribed and loaded with MCP protein. For two genes with equal rates of transcription, the brightness of foci should be proportional to the length of the 3′ UTR following transcription of the MS2 loops. Strikingly, we found that this naive model was sufficient to explain the intensity of transcriptional foci for all five IEGs (Figure 3E); burst intensity was linearly proportional to 3′ UTR length across all five IEGs tested, as would be predicted if each was transcribed with similar rates of polymerase loading, elongation, and termination. Taken together, our results suggest that IEGs share highly similar transcriptional responses, with a similar amplitude and duration of transcript production in response to a constant mitogenic stimulus.

IEG Protein Accumulation Is Regulated by Combinatorial Signaling Control

Our initial experiments revealed that IEGs exhibit strong similarities in transcriptional dynamics but divergent patterns of protein accumulation. Where might these differences arise? To address this question, we focused on Btg2, an IEG with no detectable protein accumulation in response to light. Moreover, none of the dynamic light inputs applied in this study induced Btg2-YFP accumulation, strongly suggesting that Ras temporal dynamics alone are insufficient to regulate Btg2. We thus sought to test whether different combinations of pathways might instead elicit a Btg2 response.

Btg2 is also known to be activated in contexts other than growth factor signaling; notably, its transcription is induced after DNA damage in a p53-dependent manner (Porter et al., 2016). To test whether DNA damage elicits fundamentally different

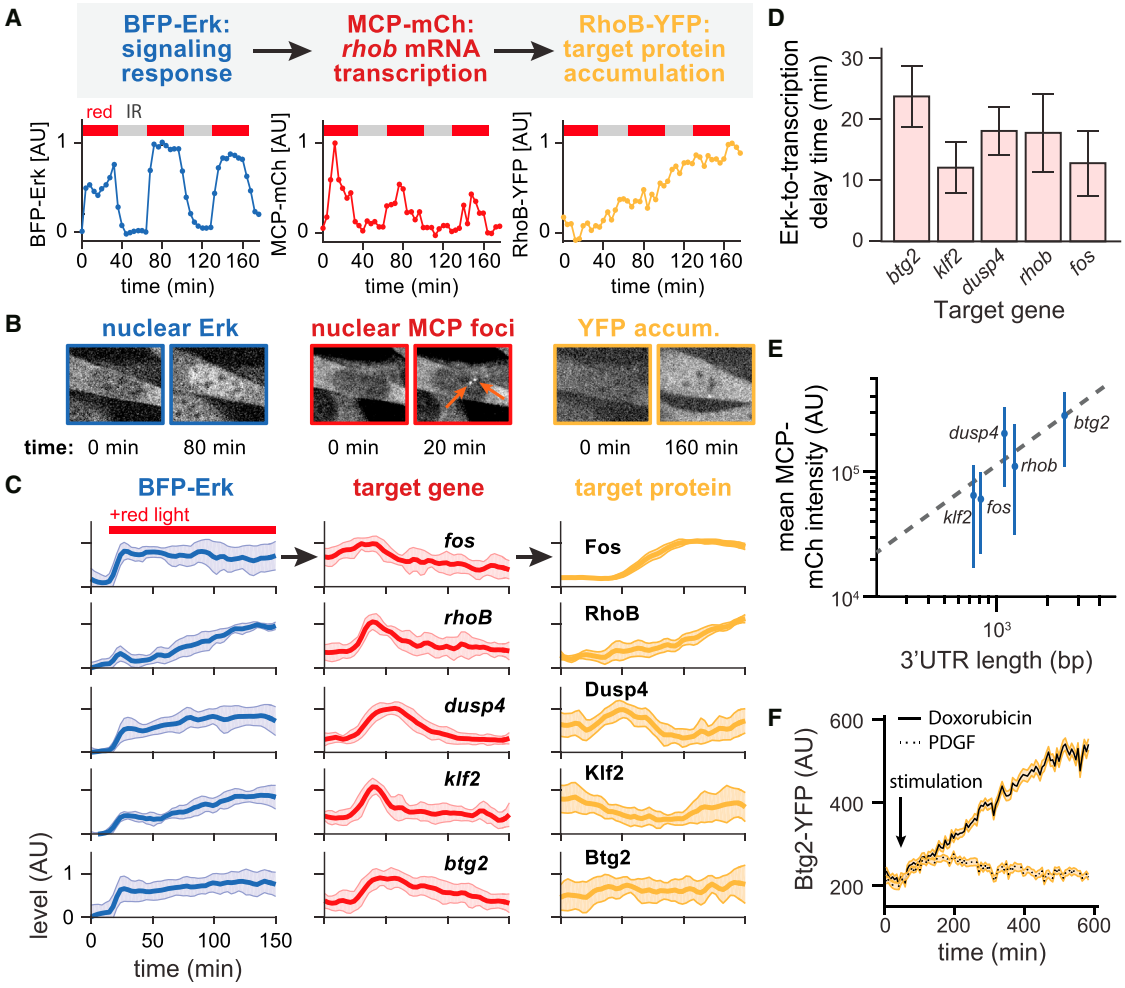

Figure 3. Visualizing Signal Transmission through the Central Dogma

(A) Nuclear BFP-Erk (left), MCP-mCherry transcriptional foci (middle), and RhoB-msfYFP protein accumulation (right) in response to a sequence of red and infrared light inputs applied to OptoSOS-RhoB cells.

(B) Representative images before and after light stimulation for the cell quantified in (A). Note the appearance of two foci (red arrows) corresponding to the *rhob* expression from both genomic loci.

(C) Sustained light stimulation of all five OptoSOS-IEG cell lines. Curves indicate mean ± SEM of nuclear BFP Erk translocation (left), MCP-mCherry nuclear focus intensity (middle), and msfYFP-IEG protein accumulation (right) from at least 20 cells per panel.

(D) Delay times (mean ± SEM) between maximum instantaneous nuclear BFP-Erk accumulation and peak target gene activation.

(E) The amplitude of transcriptional foci (mean ± SEM) after light stimulation plotted against the 3′ UTR length for each IEG. Dotted line indicates linear fit.

(F) Quantification of cytoplasmic Btg2-YFP in cells treated with Dox or PDGF. Mean ± SEM are shown.

See also Figure S3.

transcript- and protein-level dynamics, we treated OptoSOS-Btg2 cells with the DNA damaging agent doxorubicin (Dox) or PDGF. Both Dox and PDGF induced similar MCP foci, indicating *btg2* transcription, but only Dox led to the induction of Btg2-YFP at the protein level (Figure 3F). In Dox-treated cells, the levels of Btg2-YFP continued to accumulate over at least 6 hr. As Btg2 is known to be highly unstable in resting cells, with a protein half-life of less than 15 min (Mauxion et al., 2008), it is possible that DNA damage signaling acts to both activate *btg2* transcription and stabilize Btg2 protein.

The post-transcriptional regulation we observed for Btg2 led us to hypothesize that distinct cellular inputs such as growth factor stimulation and DNA damage might be differentially decoded by other IEGs as well. To further elucidate the range of computations made by IEGs, we set out to systematically compare Btg2 to the two genes that showed strong protein-level responses to PDGF: Fos and RhoB. We treated OptoSOS-Btg2, Fos, and RhoB cells with Dox, PDGF, or a cocktail of both stimuli and quantified transcription and protein accumulation. Each target gene exhibited distinct logical responses to Dox, PDGF, or their combination (Figures S3B–S3D; Movie S3). These experiments revealed cases where the mRNA- and protein-level responses were dramatically different for a single gene. For instance, we observed transcription without detectable protein

accumulation for Btg2, Dusp4, and Klf2 after light and PDGF stimulation (Figures 3C and S3C). Moreover, although PDGF and PDGF + Dox treatment led to *rhob* transcription, only PDGF induced RhoB protein accumulation (Figures S3E–S3G). Thus, despite a common transcriptional response, individual IEGs are subject to diverse post-transcriptional regulation that ensures protein-level responses are limited to specific combinations of stimuli.

Dephosphorylation of Nuclear Erk Drives Transcriptional Adaptation

We have shown that continuous Ras stimulation drives persistent Erk phosphorylation and nuclear localization but only elicits transient IEG transcription. Conversion of a persistent input to a transient response is a hallmark of adaptation, a process that is prevalent in a wide range of sensory systems (e.g., animal vision, cellular stress responses). Adaptation is thought to allow pathway responses to a wide range of input stimulus strengths (Hoeller et al., 2014). It can be achieved by a variety of detailed mechanisms but typically involves the delayed induction of a negative regulator, either in proportion to the input (thereby forming an incoherent feed-forward loop) or to the output (a negative feedback loop) (Ma et al., 2009). Many potential feedback loops have been identified that could potentially regulate Ras/Erk signaling and downstream gene expression (Amit et al., 2007), and we sought to identify whether any of these network motifs play an indispensable role in IEG transcriptional adaptation.

Based on the ~1 hr timescale of adaptation in our system, we reasoned that the negative regulator may also be an Erk target gene. We tested whether treatment with the translation inhibitor cycloheximide (CHX) could block transcriptional adaptation, focusing primarily on OptoSOS-RhoB cells. Indeed, CHX treatment completely abrogated adaptation of *rhob* transcription, leading to sustained, high-amplitude transcription over time (Figure 4A; Movie S4). Similar results were obtained from the other four target genes and also extended to dynamic stimuli. In the presence of CHX, transcriptional dynamics precisely tracked time-varying light inputs for at least 5 hr (Figures S4A and S4B). Newly synthesized negative regulators are thus sufficient to explain all of the transcriptional adaptation we observed, ruling out contributions from known post-translational feedback loops (e.g., Raf phosphorylation by Erk) or additional Ras-to-Erk feed-forward signaling.

We also tested whether the adaptation uncovered by optogenetic Ras stimulation was relevant to the physiological inputs that normally activate the Ras/Erk pathway in fibroblasts. Again focusing on the RhoB-YFP cell line, we first tested whether PDGF pretreatment could induce an adapted state that would interfere with subsequent light-induced transcription (Figure 4B). We found that PDGF induced a pulse of *rhob* transcription that, after adaptation, prevented further light-induced transcription. Conversely, pretreatment with a 90-min light pulse also prevented PDGF-induced transcription (Figure 4C). Similar results were also obtained for serum treatment, an alternative Erk-activating stimulus (Figure 4D). Our results thus demonstrate that transcriptional adaptation is a general response to sustained Ras/Erk stimuli and could serve as an integration point for comparing recent Erk-activating inputs.

We next sought to identify the molecular process targeted by this adaptation circuit. Erk-dependent negative feedback could in principle operate upstream of Erk, targeting members of the Ras/Erk cascade, or downstream, targeting Erk or the transcriptional machinery directly. However, sustained light stimulation continued to drive nuclear Erk localization even long after transcription had fully adapted, consistent with upstream signaling that does not adapt (Figure 3C). We therefore focused on downstream nodes, starting with nuclear Erk activity. Immunofluorescence imaging of doubly phosphorylated Erk (dpErk) after light stimulation revealed that nuclear Erk phosphorylation also adapted to pre-stimulus levels on the same timescale as *IEG* transcription and that adaptation was blocked by CHX pretreatment (Figures 4E and 4F). In contrast, cytoplasmic dpErk levels remained high as long as light was present and were unaffected by CHX. Similar effects on nuclear dpErk levels were also obtained when transcription was blocked by actinomycin D treatment (Figures S4C and S4D), confirming that negative feedback acts via new transcript/protein synthesis.

Our data are thus consistent with a model of organelle-specific negative feedback. A sustained input to Ras induces continuous MEK activity and phosphorylation of cytoplasmic Erk, leading to Erk nuclear translocation. Negative feedback in the nucleus (but not the cytoplasm) leads to dephosphorylation of nuclear Erk without affecting cytoplasmic MEK activity, resulting in a state with high nuclear Erk levels but low kinase activity and suppression of Erk-dependent transcription.

We hypothesized that negative feedback on nuclear Erk might depend on a well-described class of negative regulators, the dual specificity phosphatases (DUSPs). Multiple members of the DUSP family are known to dephosphorylate Erk and are also restricted to the nucleus (Caunt et al., 2008). Our RNA-seq data confirm that *dusp* genes are induced in response to Ras activation (Figures S4E and S4F), thereby forming a putative negative feedback loop. To further test this model, we used a mutant allele of Erk (ErkD319N) known to confer insensitivity to DUSPs (Brunner et al., 1994; Caunt et al., 2008). We transduced OptoSOS-RhoB cells with similar expression levels of BFP-Erk or BFP-ErkD319N (Figure S4G) and monitored light-induced *rhob* transcription and RhoB-YFP protein levels. When compared to unmutated Erk, light-stimulated ErkD319N cells showed a higher overall amplitude of *rhob* transcription and did not completely adapt, leading to persistent puncta of nuclear MCP (Figure 4G; Movie S5). We also observed higher levels of RhoB-YFP accumulation in ErkD319N-expressing cells (Figure S4H).

Despite their persistent transcriptional response, some adaptation was still present in D319N cells. This residual adaptation could be explained in three ways: (1) our cells express ErkD319N on top of endogenous Erk1 and Erk2, which could still be targeted by DUSPs, (2) the D319N mutation may only partly block DUSP binding, and (3) additional negative regulators of nuclear Erk may also contribute to adaptation. Nevertheless, our results demonstrate that Erk-dependent DUSP phosphatase activity plays at least a partial role in limiting the duration of IEG transcription, providing one mechanism for ensuring transient IEG transcription despite sustained MAPK pathway activation (Figure 4H).

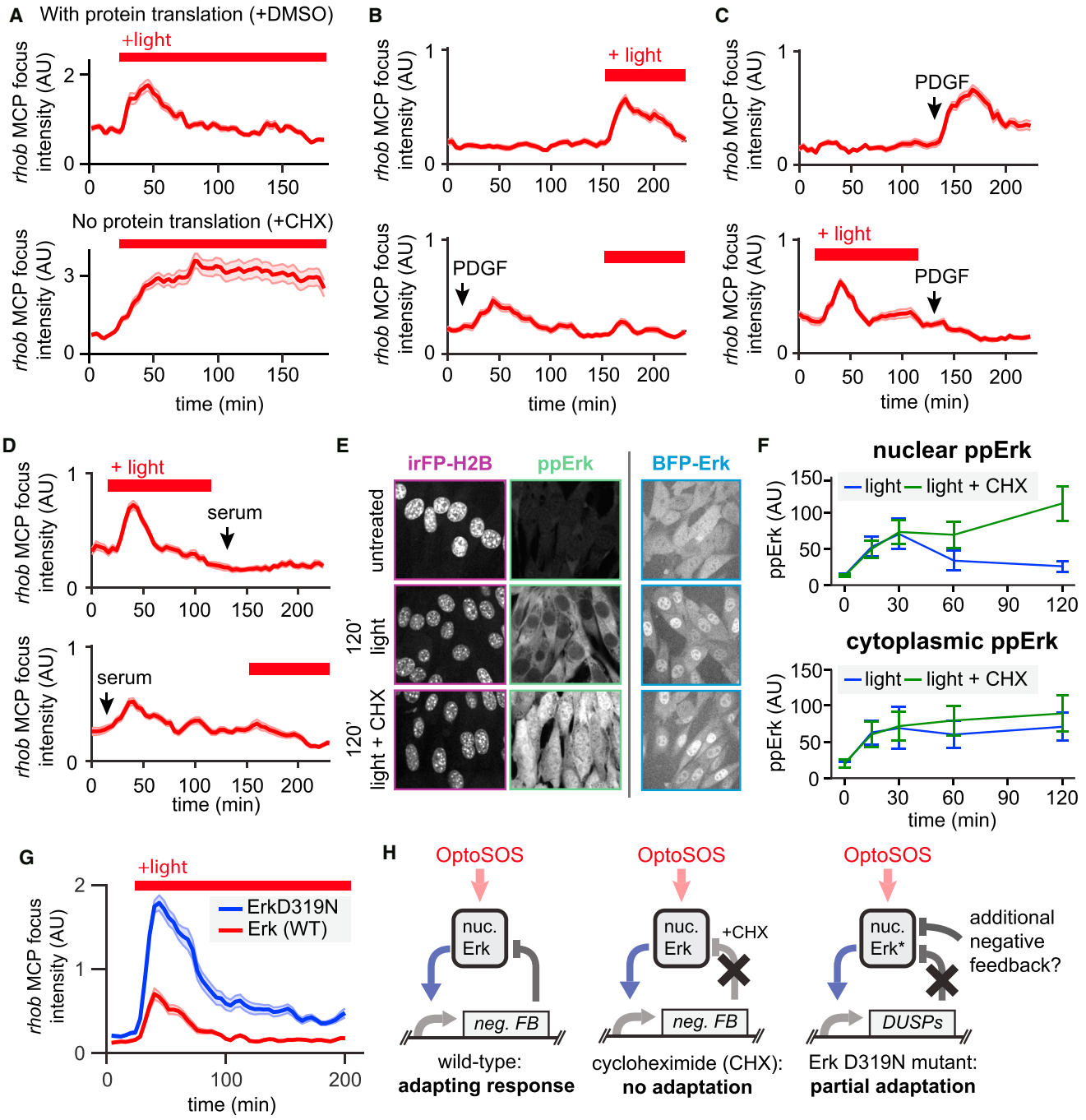

Figure 4. Organelle-Specific Dephosphorylation of Nuclear Erk Drive Transcriptional Adaptation

(A–D) Quantification of MCP-mCherry nuclear foci (mean ± SEM) over time in OptoSOS-RhoB cells after light stimulation. Cells were stimulated with cycloheximide (CHX) or vehicle control (A), light with or without pre-treatment with PDGF (B), PDGF with or without pretreatment with light (C), and sequential stimulation with light and 10% fetal bovine serum (D).

(E) Images of dpErk localization in the OptoSOS chassis cell line after light stimulation and in the presence or absence of CHX. Images show fluorescent histone H2B-diRFP (left), antibody staining for dpErk (middle), and BFP-Erk2 localization (right).

(F) Nuclear and cytoplasmic dpErk quantified over time after light stimulation (mean ± SEM), with or without CHX.

(G) MCP-mCherry nuclear focus intensity (mean ± SEM) in cells transduced with BFP-Erk2 D319N (blue) or BFP-Erk2 (red).

(H) Negative feedback on nuclear Erk can be blocked by translation inhibition and reduced by expression of Erk D319N.

See also Figure S4.

Adaptation of IEG Transcription Implements Bandpass Filtering of Erk Dynamics

Our studies have so far implicated negative feedback in limiting IEG output in response to constant, sustained Erk inputs. However, more complex Erk dynamics have been observed in experimental systems ranging from cultured epithelial cells (Albeck et al., 2013) to primary cells in live mice (Hiratsuka et al., 2015). Some evidence suggests that Erk target genes may be selectively transcribed in response to certain dynamic stimuli, although the mechanisms underlying dynamic filtering are still unknown (Aoki et al., 2013). How might transcriptional adaptation affect responses to the Erk dynamics observed in diverse natural contexts?

To address this question, we first built a mathematical model focused on three central processes: activation of Erk by upstream inputs, feedback inhibition on nuclear Erk, and Erk-induced transcription of target genes. Our model consists of four equations representing Erk, *dusp* transcripts, DUSP protein (which represent both DUSPs and any other putative Erk-dependent negative regulators), and transcription of a representative target IEG (Figure 5A; STAR Methods; Data S1). We set out to use this model as a simple and concise framework for investigating how MAPK pathway dynamics might affect the magnitude of IEG responses.

We focused primarily on simulating inputs that are reminiscent of the experimentally observed endogenous Erk activity pulses, which typically last for ~20 min and occur with a time between pulses that varies with cellular context, ranging from ~30 min to ~4 hr (Albeck et al., 2013; Aoki et al., 2013). We applied inputs with a constant 20-min t_{ON} but variable t_{OFF} (Figures 5B and 5C). Continuous stimulation (t_{OFF} = 0 min) drove adaptation in target transcription due to induction of negative feedback, similar to that observed experimentally (Figure 5B, top). In contrast, recurrent input pulses (t_{OFF} = 64 min) were much more efficient, leading to repeated pulses of target transcription without triggering adaptation (Figure 5B, bottom). Our results were highly sensitive to t_{OFF}; too much time between pulses and transcription was inefficient, whereas too little and adaptation led to a damping envelope that reduced the response amplitude of later pulses (Figure 5C). Thus, the model predicts that an intermediate stimulus frequency can drive maximum IEG expression, the hallmark response of band-pass filtering.

We next tested whether bandpass filtering might be altered by parameters that could vary between target genes. We found that the parameter K_i, which represents the level of Erk required to induce half-maximal transcript production, is a critical determinant of dynamic filtering (Figure 5D). For promoters with high Erk sensitivity (low K_i), simulations revealed that even the low Erk activity reached after adaptation could induce a transcriptional response. High-sensitivity promoters would thus be expected to respond to constant stimuli and act as low-pass filters of Erk dynamics (Figure 5D, light blue). In contrast, band-pass filtering was predicted for promoters with low to intermediate Erk sensitivity (i.e., intermediate-high values of K_i). In this regime, the optimal stimulus frequency varied with a gene's Erk sensitivity (Figure 5D). Notably, a wide range of Ras/Erk dynamics have been observed experimentally, with t_{OFF} ranging from 15 minutes to multiple hours (Albeck et al., 2013; Shankaran et al., 2009). As expected, we found that negative feedback was necessary for adaptation and band-pass filtering. A second parameter, mRNA stability, was predicted to have no effect on dynamic filtering (Figures S5A and S5B). Our computational results thus demonstrate that a remarkably simple model, Erk adaptation coupled to target promoters with varying Erk sensitivity, could relay these different naturally occurring Erk dynamics to distinct sets of target genes.

We next set out to compare our model results to experimental IEG induction profiles. We first tested whether recurrent input pulses could indeed drive multiple rounds of transcription without triggering adaptation. We stimulated OptoSOS-RhoB cells with 20-min activating red light pulses separated by 20-min periods of deactivating infrared light and monitored *rhob* transcription. We observed repeated pulses of *rhob* transcription that tracked our light input for at least 5 hr, confirming that Erk pulses can repeatedly activate IEG transcription without triggering complete adaptation (Figure 5E; Movie S6). We next tested if all 5 IEGs were band-pass filtered by measuring their responses across a range of dynamic light stimuli. We delivered 20-min pulses of activating light separated by periods of deactivating light (t_{OFF}) ranging from 4 to 334 min. We found that 4 of 5 genes exhibited clear maximal responses at intermediate input pulse frequencies, with *klf2* exhibiting a weaker frequency-selective response. Interestingly, the optimal frequency of stimulation varied between IEGs (Figures 5F and S5C), with *dusp4* and *btg2* sharing a peak output (t_{OFF} = 128 min) and *fos*/*rhob* exhibiting different maximum responses (t_{OFF} = 32 min and 64 min, respectively). Bandpass filtering was also evident at the protein level for Fos-YFP (Figures S5D and S5E). We thus conclude that IEGs can act as tunable band-pass filters of upstream stimulus dynamics. More broadly, our results reveal that a rich set of signals can be transmitted through the Ras/Erk pathway and processed to induce dynamics-sensitive gene expression.

DISCUSSION

The OptoSOS System: Tracing Signal Flow through the Central Dogma in Live Cells

The development of live cell biosensors at multiple intracellular nodes is revolutionizing our understanding of the fundamental dynamics governing cell signaling (Purvis and Lahav, 2013), transcription (Larson et al., 2011), and translation (Wu et al., 2016). However, despite an increasingly detailed picture *within* each level, we are only beginning to understand how information is propagated *between* them. Here, we set out to implement an end-to-end system for dissecting information flow through a signaling pathway to the nucleus and then back out through the central dogma for specific target genes.

Based on our data, we propose a two-tiered scheme by which upstream signaling regulates IEG accumulation (Figure 6). At the transcriptional level, we find that the production of *IEG* mRNA is dynamically gated. Repeated pulses of Erk activity drive multiple cycles of transcription, whereas sustained or infrequent inputs induce lower levels of transcription. Modeling and experimental data indicate that dynamic filtering can be regulated in a

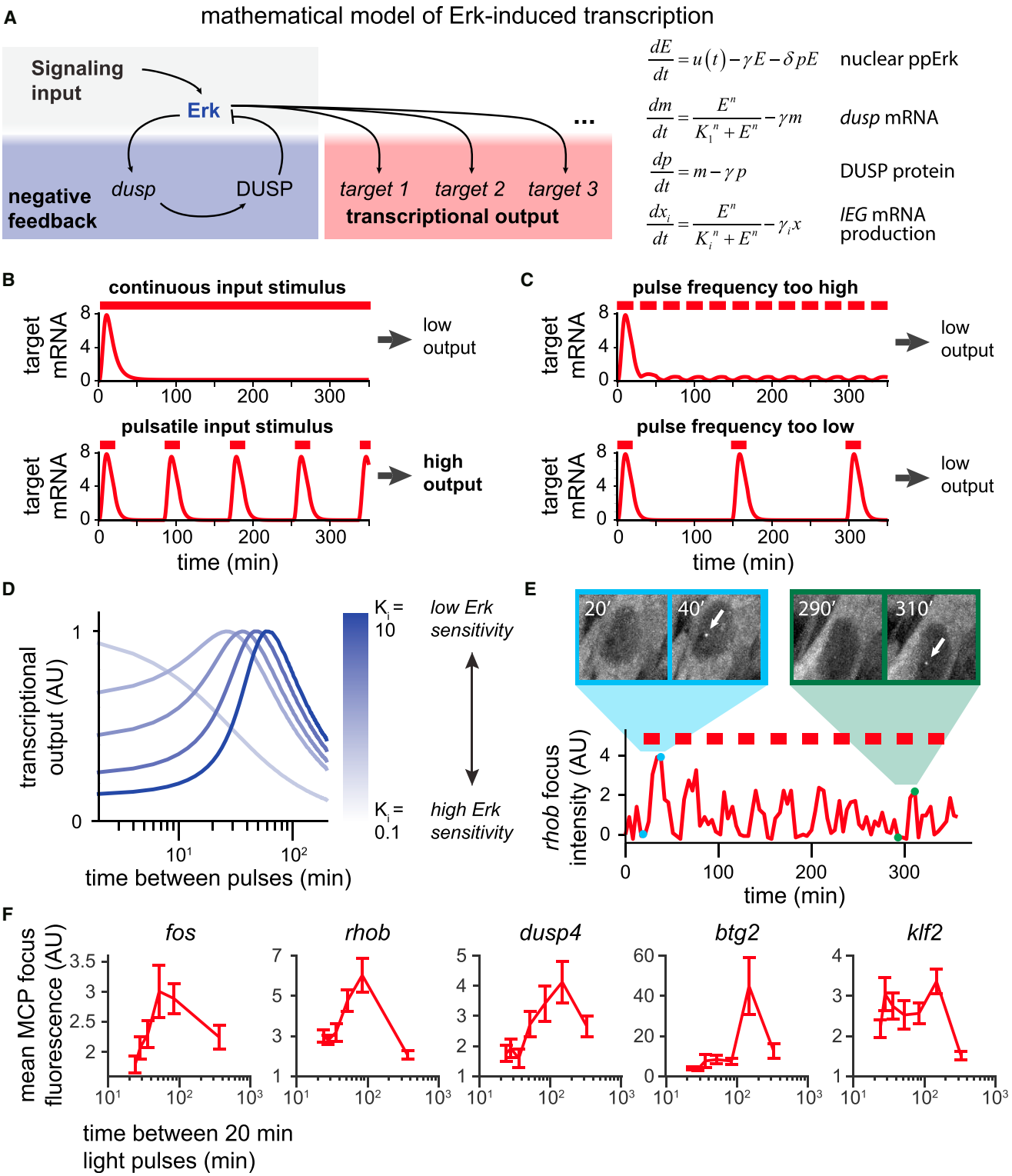

Figure 5. Adaptation of IEG Transcription Implements a Bandpass Filter of Dynamic Erk Activity

(A) Mathematical model of Erk-induced transcription. Schematic representation of interactions simulated using equations representing nuclear dpErk, *dusp* mRNA, Dusp protein, and *IEG* transcripts with differing sensitivities to Erk.

(B) Simulations showing adaptation of transcription under continuous light (top) but repeated bouts of transcription in response to intermittent light pulses (bottom).

(legend continued on next page)

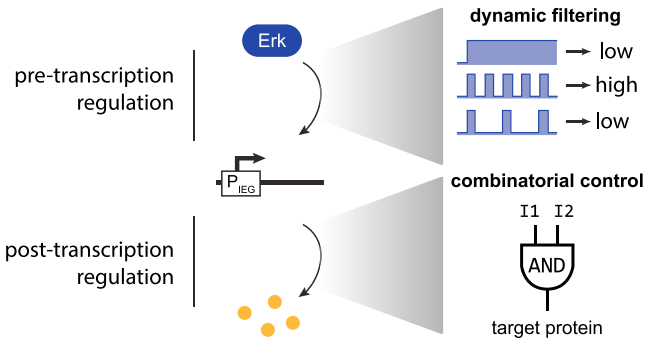

Figure 6. IEGs Are Regulated by Dynamic and Combinatorial Control
Our study suggests a two-tiered scheme for IEG regulation. First, *IEG* transcription is dynamically controlled by the Ras/Erk pathway. Long-term Erk inputs lead to adaptation of *IEG* transcription, whereas periodic Erk stimuli lead to repeated cycles of transcriptional induction. Second, IEG protein production is combinatorially controlled. Two stimuli that both elicit transcription can have differential protein-level outcomes, demonstrating that different pathway inputs control both transcriptional and post-transcriptional steps.

gene-specific manner, leading to different amounts of transcript production even for a single dynamic input stimulus.

We also find evidence for a second level of regulation, acting post-transcriptionally, that controls which IEGs are produced in response to extracellular cues. Despite similar transcription profiles, many IEGs do not accumulate at the protein level after light-activated Ras or PDGF stimulation. Moreover, IEG protein accumulation can be induced or suppressed by specific combination of signaling cues. For instance, although *rhob* is always transcribed in response to growth factor treatment, RhoB protein induction appears to evaluate the logical expression "growth factor AND NOT DNA damage." Our observations thus suggest that even for a classic signaling-to-gene-expression system like the growth factor control of IEGs, rich layers of regulation remain to be uncovered and mechanistically understood.

The two-tiered regulatory scheme we propose might enable cells to combine information encountered by the cell on very different timescales (Gordley et al., 2016). On a slow timescale, transcript accumulation could respond to multiple cycles of dynamic pathway activity, enabling cells to integrate information about environmental conditions (e.g., whether the cell's environment is permissive for growth) over periods of multiple hours. In contrast, a fast layer of post-transcriptional combinatorial control could enable cells to rapidly transduce information from additional input pathways (e.g., the acute presence of cellular stress) into a protein-level response, taking advantage of transcripts that have already integrated long-timescale information.

A Pulse Generator Links Erk Dynamics to Target Gene Transcription

The observation of band-pass filtering at the transcriptional level could have far-reaching consequences for understanding how information is transmitted from the Ras/Erk pathway to target gene induction. Rather than focusing solely on model cellular contexts where Erk activity is thought to be either transient or sustained, our work points to the importance of the pulsatile Erk dynamics that have now been observed across a wide range of contexts both in vitro (Albeck et al., 2013; Aoki et al., 2013; Shankaran et al., 2009) and in vivo (Hiratsuka et al., 2015; Kumagai et al., 2015). Moreover, we found that the enrichment of Erk in the nucleus does not necessarily imply a high level of nuclear Erk activity. Such organelle-specific regulation provides an elegant solution to the challenge of decoupling the multiple roles of Erk within the cell, enabling the dynamic regulation of target genes without affecting Erk substrate phosphorylation in other cellular compartments. Our results also highlight the importance of biosensors that report directly on kinase activity, not just protein localization (Regot et al., 2014).

Why might a pathway encode information in a temporal sequence of pulses rather than in the amplitude or duration of a constant stimulus? One possible reason may relate to the role of Ras/Erk signaling in disease. Cancer and many developmental disorders are thought to rely on enhanced signaling through the Ras/Erk pathway to drive improper proliferation or differentiation (Johnson et al., 2017). We would predict that oncogenic Ras pathway mutations (e.g., at EGFR, Ras, or Raf) would induce nuclear Erk activity that would still be subject to DUSP-mediated adaptation and thus drive a brief transcriptional pulse, providing a valuable brake on sustained growth-promoting gene activation. This model would imply that nuclear-localized, Erk-specific DUSPs play a crucial role in suppressing Erk-dependent transcription in response to activating Ras pathway mutations and function as important tumor suppressors, as has recently been reported (Balko et al., 2013; Rushworth et al., 2014).

A second reason that temporal encoding may be advantageous is that it could enable a single pathway to be repurposed to differentially regulate target genes. Our model demonstrates that a remarkably simple network—a single negative feedback loop coupled to target gene promoters with different sensitivities to Erk—enables target genes to act as tunable band-pass filters that respond to specific frequencies of Ras pulses. The frequency of upstream stimuli may thus be decoded into distinct cellular responses, consistent with recent studies showing that pulsatile nerve growth factor (NGF) stimulation induces more homogeneous differentiation in PC-12 cells than does continuous stimulation (Ryu et al., 2016), as well as by

(C) Simulations showing decreased transcription if the frequency of light pulses is too high (top) or low (bottom).
(D) Simulated total transcript production as a function of t_{OFF} for target genes with different sensitivities to Erk (K_i). Each curve is normalized to its peak output.
(E) Images of transcriptional foci (top; white arrows) and quantified MCP-mCherry nuclear focus intensity (bottom) of a representative OptoSOS-RhoB cell demonstrating repeated responses to optimally spaced input pulses.
(F) Quantification of MCP-mCherry nuclear focus intensity (mean ± SEM) during time courses as in (E), where cells were subjected to 20 min activating light pulses separated by inactivating light pulses lasting from 4 to 384 min.
See also Figure S5.

the finding that certain frequencies of osmolarity stress dramatically reduce yeast cell growth (Mitchell et al., 2015). Future studies combining precise optogenetic stimuli and reporters of cell fate could shed new light on whether the dynamics of a single pathway are sufficient to distinguish among cell fate responses.

STAR★METHODS

Detailed methods are provided in the online version of this paper and include the following:

- KEY RESOURCES TABLE
- CONTACT FOR REAGENT AND RESOURCE SHARING
- METHOD DETAILS
  - Cell culture
  - RNA sequencing
  - Lentivirus production and transduction
  - Generation of clonal chassis cell line
  - CRISPR integration and isolation of native loci tagged IEGs
  - Cell preparation prior to imaging
  - Imaging
  - Optogenetic stimulation hardware
  - Quantification of transcriptional foci
  - Drug treatment
  - Immunofluorescence staining
- CELL LYSATE COLLECTION/WESTERN BLOTS
  - Mathematical model of Erk-to-transcription dynamic transmission
- QUANTIFICATION AND STATISTICAL ANALYSIS
- DATA AND SOFTWARE AVAILABILITY

SUPPLEMENTAL INFORMATION

Supplemental Information includes five figures, six movies, and one dataset and can be found with this article online at http://dx.doi.org/10.1016/j.molcel.2017.07.016.

AUTHOR CONTRIBUTIONS

Conceptualization, M.Z.W. and J.E.T.; Methodology, M.Z.W. and J.E.T.; Investigation, M.Z.W., P.T.R., and J.E.T.; Writing – Original Draft, M.Z.W. and J.E.T.; Writing – Review & Editing, M.Z.W., P.T.R., and J.E.T.; Funding Acquisition, M.Z.W., W.A.L. and J.E.T.; Resources, W.A.L. and J.E.T.; Supervision, J.E.T.

ACKNOWLEDGMENTS

We thank all members of the Toettcher lab for helpful comments. This work was supported by NIH grant DP2EB024247 (to J.E.T.), an Innovation Award from the New Jersey Health Foundation (to M.Z.W.), and the Howard Hughes Medical Institute and NIH grant P50GM081879, to W.A.L. We also thank Dr. Gary Laevsky and the Princeton Molecular Biology Microscopy Core for microscopy support, Dr. Christina DeCoste and the Princeton Molecular Biology Flow Cytometry Resource Center for cell sorting, and the UCSF Center for Advanced Technology for sequencing support.

Received: March 1, 2017
Revised: June 12, 2017
Accepted: July 13, 2017
Published: August 17, 2017

REFERENCES

Albeck, J.G., Mills, G.B., and Brugge, J.S. (2013). Frequency-modulated pulses of ERK activity transmit quantitative proliferation signals. Mol. Cell *49*, 249–261.

Amit, I., Citri, A., Shay, T., Lu, Y., Katz, M., Zhang, F., Tarcic, G., Siwak, D., Lahad, J., Jacob-Hirsch, J., et al. (2007). A module of negative feedback regulators defines growth factor signaling. Nat. Genet. *39*, 503–512.

Aoki, K., Kumagai, Y., Sakurai, A., Komatsu, N., Fujita, Y., Shionyu, C., and Matsuda, M. (2013). Stochastic ERK activation induced by noise and cell-to-cell propagation regulates cell density-dependent proliferation. Mol. Cell *52*, 529–540.

Balko, J.M., Schwarz, L.J., Bhola, N.E., Kurupi, R., Owens, P., Miller, T.W., Gómez, H., Cook, R.S., and Arteaga, C.L. (2013). Activation of MAPK pathways due to DUSP4 loss promotes cancer stem cell-like phenotypes in basal-like breast cancer. Cancer Res. *73*, 6346–6358.

Bishop, J.M., Capobianco, A.J., Doyle, H.J., Finney, R.E., McMahon, M., Robbins, S.M., Samuels, M.L., and Vetter, M. (1994). Proto-oncogenes and plasticity in cell signaling. Cold Spring Harb. Symp. Quant. Biol. *59*, 165–171.

Brunner, D., Oellers, N., Szabad, J., Biggs, W.H., 3rd, Zipursky, S.L., and Hafen, E. (1994). A gain-of-function mutation in Drosophila MAP kinase activates multiple receptor tyrosine kinase signaling pathways. Cell *76*, 875–888.

Caunt, C.J., Armstrong, S.P., Rivers, C.A., Norman, M.R., and McArdle, C.A. (2008). Spatiotemporal regulation of ERK2 by dual specificity phosphatases. J. Biol. Chem. *283*, 26612–26623.

Darzacq, X., Yao, J., Larson, D.R., Causse, S.Z., Bosanac, L., de Turris, V., Ruda, V.M., Lionnet, T., Zenklusen, D., Guglielmi, B., et al. (2009). Imaging transcription in living cells. Annu. Rev. Biophys. *38*, 173–196.

Garcia, H.G., Tikhonov, M., Lin, A., and Gregor, T. (2013). Quantitative imaging of transcription in living Drosophila embryos links polymerase activity to patterning. Curr. Biol. *23*, 2140–2145.

Giardine, B., Riemer, C., Hardison, R.C., Burhans, R., Elnitski, L., Shah, P., Zhang, Y., Blankenberg, D., Albert, I., Taylor, J., et al. (2005). Galaxy: a platform for interactive large-scale genome analysis. Genome Res. *15*, 1451–1455.

Gordley, R.M., Williams, R.E., Bashor, C.J., Toettcher, J.E., Yan, S., and Lim, W.A. (2016). Engineering dynamical control of cell fate switching using synthetic phospho-regulons. Proc. Natl. Acad. Sci. USA *113*, 13528–13533.

Grimm, O., Sanchez Zini, V., Kim, Y., Casanova, J., Shvartsman, S.Y., and Wieschaus, E. (2012). Torso RTK controls Capicua degradation by changing its subcellular localization. Development *139*, 3962–3968.

Guzowski, J.F., McNaughton, B.L., Barnes, C.A., and Worley, P.F. (1999). Environment-specific expression of the immediate-early gene Arc in hippocampal neuronal ensembles. Nat. Neurosci. *2*, 1120–1124.

Hannanta-Anan, P., and Chow, B.Y. (2016). Optogenetic control of calcium oscillation waveform defines NFAT as an integrator of calcium load. Cell Syst. *2*, 283–288.

Hiratsuka, T., Fujita, Y., Naoki, H., Aoki, K., Kamioka, Y., and Matsuda, M. (2015). Intercellular propagation of extracellular signal-regulated kinase activation revealed by in vivo imaging of mouse skin. eLife *4*, e05178.

Hoeller, O., Gong, D., and Weiner, O.D. (2014). How to understand and outwit adaptation. Dev. Cell *28*, 607–616.

Johnson, H.E., Goyal, Y., Pannucci, N.L., Schüpbach, T., Shvartsman, S.Y., and Toettcher, J.E. (2017). The spatiotemporal limits of developmental Erk signaling. Dev. Cell *40*, 185–192.

Klinghoffer, R.A., Hamilton, T.G., Hoch, R., and Soriano, P. (2002). An allelic series at the PDGFalphaR locus indicates unequal contributions of distinct signaling pathways during development. Dev. Cell *2*, 103–113.

Kumagai, Y., Naoki, H., Nakasyo, E., Kamioka, Y., Kiyokawa, E., and Matsuda, M. (2015). Heterogeneity in ERK activity as visualized by in vivo FRET imaging of mammary tumor cells developed in MMTV-Neu mice. Oncogene *34*, 1051–1057.

Larson, D.R., Zenklusen, D., Wu, B., Chao, J.A., and Singer, R.H. (2011). Real-time observation of transcription initiation and elongation on an endogenous yeast gene. Science *332*, 475–478.

Ma, W., Trusina, A., El-Samad, H., Lim, W.A., and Tang, C. (2009). Defining network topologies that can achieve biochemical adaptation. Cell *138*, 760–773.

Mangan, S., and Alon, U. (2003). Structure and function of the feed-forward loop network motif. Proc. Natl. Acad. Sci. USA *100*, 11980–11985.

Marshall, C.J. (1995). Specificity of receptor tyrosine kinase signaling: transient versus sustained extracellular signal-regulated kinase activation. Cell *80*, 179–185.

Mauxion, F., Faux, C., and Séraphin, B. (2008). The BTG2 protein is a general activator of mRNA deadenylation. EMBO J. *27*, 1039–1048.

Miller, A.D., Curran, T., and Verma, I.M. (1984). c-fos protein can induce cellular transformation: a novel mechanism of activation of a cellular oncogene. Cell *36*, 51–60.

Mitchell, A., Wei, P., and Lim, W.A. (2015). Oscillatory stress stimulation uncovers an Achilles' heel of the yeast MAPK signaling network. Science *350*, 1379–1383.

Mori, S., Heldin, C.H., and Claesson-Welsh, L. (1992). Ligand-induced polyubiquitination of the platelet-derived growth factor beta-receptor. J. Biol. Chem. *267*, 6429–6434.

Murphy, L.O., Smith, S., Chen, R.H., Fingar, D.C., and Blenis, J. (2002). Molecular interpretation of ERK signal duration by immediate early gene products. Nat. Cell Biol. *4*, 556–564.

Pédelacq, J.D., Cabantous, S., Tran, T., Terwilliger, T.C., and Waldo, G.S. (2006). Engineering and characterization of a superfolder green fluorescent protein. Nat. Biotechnol. *24*, 79–88.

Porter, J.R., Fisher, B.E., and Batchelor, E. (2016). p53 pulses diversify target gene expression dynamics in an mRNA half-life-dependent manner and delineate co-regulated target gene subnetworks. Cell Syst. *2*, 272–282.

Purvis, J.E., and Lahav, G. (2013). Encoding and decoding cellular information through signaling dynamics. Cell *152*, 945–956.

Regot, S., Hughey, J.J., Bajar, B.T., Carrasco, S., and Covert, M.W. (2014). High-sensitivity measurements of multiple kinase activities in live single cells. Cell *157*, 1724–1734.

Rushworth, L.K., Kidger, A.M., Delavaine, L., Stewart, G., van Schelven, S., Davidson, J., Bryant, C.J., Caddye, E., East, P., Caunt, C.J., and Keyse, S.M. (2014). Dual-specificity phosphatase 5 regulates nuclear ERK activity and suppresses skin cancer by inhibiting mutant Harvey-Ras (HRasQ61L)-driven SerpinB2 expression. Proc. Natl. Acad. Sci. USA *111*, 18267–18272.

Ryu, H., Chung, M., Dobrzyński, M., Fey, D., Blum, Y., Sik Lee, S., Peter, M., Kholodenko, B.N., Li Jeon, N., and Pertz, O. (2016). Frequency modulation of ERK activation dynamics rewires cell fate. Mol. Syst. Biol. *12*, 866.

Senecal, A., Munsky, B., Proux, F., Ly, N., Braye, F.E., Zimmer, C., Mueller, F., and Darzacq, X. (2014). Transcription factors modulate c-Fos transcriptional bursts. Cell Rep. *8*, 75–83.

Shankaran, H., Ippolito, D.L., Chrisler, W.B., Resat, H., Bollinger, N., Opresko, L.K., and Wiley, H.S. (2009). Rapid and sustained nuclear-cytoplasmic ERK oscillations induced by epidermal growth factor. Mol. Syst. Biol. *5*, 332.

Stewart-Ornstein, J., and Lahav, G. (2016). Dynamics of CDKN1A in single cells defined by an endogenous fluorescent tagging toolkit. Cell Rep. *14*, 1800–1811.

Toettcher, J.E., Weiner, O.D., and Lim, W.A. (2013). Using optogenetics to interrogate the dynamic control of signal transmission by the Ras/Erk module. Cell *155*, 1422–1434.

Tullai, J.W., Schaffer, M.E., Mullenbrock, S., Sholder, G., Kasif, S., and Cooper, G.M. (2007). Immediate-early and delayed primary response genes are distinct in function and genomic architecture. J. Biol. Chem. *282*, 23981–23995.

Wu, B., Eliscovich, C., Yoon, Y.J., and Singer, R.H. (2016). Translation dynamics of single mRNAs in live cells and neurons. Science *352*, 1430–1435.

Xue, W., Chen, S., Yin, H., Tammela, T., Papagiannakopoulos, T., Joshi, N.S., Cai, W., Yang, G., Bronson, R., Crowley, D.G., et al. (2014). CRISPR-mediated direct mutation of cancer genes in the mouse liver. Nature *514*, 380–384.

Zwang, Y., Sas-Chen, A., Drier, Y., Shay, T., Avraham, R., Lauriola, M., Shema, E., Lidor-Nili, E., Jacob-Hirsch, J., Amariglio, N., et al. (2011). Two phases of mitogenic signaling unveil roles for p53 and EGR1 in elimination of inconsistent growth signals. Mol. Cell *42*, 524–535.

STAR★METHODS

KEY RESOURCES TABLE

REAGENT or RESOURCE	SOURCE	IDENTIFIER
Antibodies		
GFP rabbit antibody	Sigma-Aldrich	Cat# G1544
Total Erk 1/2 rabbit antibody	Cell Signaling Technologies	Cat# 4696S
Phospho-Erk 1/2 rabbit antibody	Cell Signaling Technologies	Cat# 4370S
Bacterial and Virus Strains		
One Shot Stbl3 Chemically Competent *E. coli*	Life Technologies	Cat# C737303
Stellar Chemically Competent Cells	Clontech Laboratories	Cat# 636763
Chemicals, Peptides, and Recombinant Proteins		
Actinomycin D	Sigma-Aldrich	Cat# A1410
CloneAmp HiFi PCR Polymerase	Clontech Laboratories	Cat# 639298
cOmplete, Mini, EDTA-free Protease Inhibitor Cocktail	Sigma-Aldrich	Cat# 11836170001
Cycloheximide	Sigma-Aldrich	Cat# C104450
Doxorubicin	AK Scientific	Cat# E518
Fugene HD	Promega	Cat# E2311
Gibson Assembly master mix and buffer	New England Biosciences	Cat# E2611L
Hygromycin B	Life Technologies	10687-010
Lipofectamine LTX with Plus Reagent	Thermo-Fisher	Cat# 15338100
NuPAGE LDS Sample Buffer	Thermo-Fisher	Cat# NP0007
PDGF BB	Thermo-Fisher	Cat# 520BB050
PhosSTOP	Sigma-Aldrich	Cat# 4906837001
Phycocyanobillin	Frontier Scientific	Cat# P14137
PrimeSTAR GXL DNA Polymerase	Clontech Laboratories	Cat# R050B
Puromycin dihydrochloride (Puromycin)	Sigma-Aldrich	Cat# P8833
QuickExtract DNA Extraction Solution	Epicenter Bio	Cat# QE09050
Critical Commercial Assays		
TruSeq RNA library preparation kit, Set A	Illumina	Cat# RS-122-2001
Deposited Data		
Raw/analyzed RNA-seq data from OptoSOS cells stimulated with light or PDGF (Figures 1 and S1)	This paper; NCBI GEO database	GEO accession # GSE100816
Experimental Models: Cell Lines		
NIH 3T3 cells	American Type Culture Collection (ATCC)	Cat# CRL-1658
Lenti-X 293 cells	Clontech Laboratories	Cat# 632180
"Chassis" cell line (NIH 3T3 + Phy-CAAX + irFP-PIF-SOS2cat + H2B-diRFP + MCP-mCherry)	This paper	Available upon request
Oligonucleotides		
Btg2 gRNA sequence: AGATAGGAGCCACCCGACCC	This paper	N/A
Dusp4 gRNA sequence: CAGCTGTTAGGACTCGTCTC	This paper	N/A
Fos gRNA sequence: GCTCACAGGGCCAGCAGCGT	This paper	N/A
Klf2 gRNA sequence: ACATGTAGCCTGGGTCGACT	This paper	N/A
RhoB gRNA sequence: AACTGCTGCAAGGTGCTATG	This paper	N/A
Recombinant DNA		
gRNA plasmids	This paper	Addgene # forthcoming
Homology plasmids (pAAV-upstream gene homology – msfYFP-24xMS2-downstream gene homology)	This paper	Addgene # forthcoming

(*Continued on next page*)

Continued

REAGENT or RESOURCE	SOURCE	IDENTIFIER
pHR SFFVp BFP-Erk	Toettcher et. al., 2013	Addgene # 50848
pHR SFFVp BFP-Erk D319N	This paper	Addgene # forthcoming
pHR SFFVp MCP-mCherry IRES h2b-diRFP	This paper	Addgene # forthcoming
pPBJ SFFVp Phy-Caax IRES BFP-Erk IRES iRFP-PIF-SOScat pCMV puro	This paper	Addgene # forthcoming
pCMV-dR8.91 lenti helper plasmid	Gift from the Trono lab	
pMD2.G lenti helper plasmid	Gift from the Trono lab	Addgene #12259
Software and Algorithms		
Fiji		http://fiji.sc
Galaxy next-generation sequencing (NGS) data analysis server, run on the Amazon cloud	Giardine et al., 2005	https://usegalaxy.org
Python Code for Model	This paper	Supplement

CONTACT FOR REAGENT AND RESOURCE SHARING

Further information and requests for resources and reagents should be directed to and will be fulfilled by the Lead Contact, Jared Toettcher, (toettcher@princeton.edu).

METHOD DETAILS

Cell culture

NIH 3T3 mouse embryonic fibroblasts were grown in DMEM supplemented with 10% FBS. Cells were maintained on Thermo Scientific Nunc Cell Culture Treated Flasks with Filter Caps and grown at 37°C with 5% CO_2. The number of passages of any cell line was limited to 10. For cell lines expressing puromycin and/or hygromycin resistance genes media was supplemented with 50 μg/ml hygromycin and/or 1 μg/ml puromycin.

RNA sequencing

NIH 3T3 OptoSOS cells were starved overnight and stimulated with PDGF or light for the appropriate time. Total RNA was collected by TRIzol treatment followed by isopropanol precipitation. mRNA purification and cDNA library preparation were performed using the TruSeq mRNA library preparation kit (Illumina), resulting in a single pooled cDNA library of barcoded samples from all stimulus conditions. The quality of the cDNA library from each experimental condition was separately assessed by Agilent Bioanalyzer. After pooling equal quantities of each barcoded sample, 50 bp reads were collected on 3 lanes of an Illumina HiSeq 2000.

Sequenced reads were trimmed for adaptor sequence and masked for low-complexity or low-quality sequences. All reads from the same index (e.g., the same experimental condition) were pooled from all 3 lanes, resulting in a total of 30-50 million reads per condition. Any remaining ribosomal/tRNA reads were excluded by first using Bowtie to map to an rRNA/tRNA genome, and discarding any successfully mapped reads. Non-ribosomal/tRNA reads were then mapped using Tophat using the mm9 genome and mouse genome annotation file (GTF) from Illumina's iGenomes page. Cufflinks/Cuffcompare was then used to generate a tracking file to compare transcript abundance (FPKM values) across all samples.

Baseline transcript abundance was measured in biological triplicate (0 min controls) and each successive time point was measured in a single experiment. Genes were considered upregulated if they were induced at least 5-fold in at least two consecutive time points relative to their baseline abundance.

Lentivirus production and transduction

Lentivirus was produced as per the protocol described in Toettcher et al. (2013). Briefly, Lenti-X 293T cells were plated in a 6-well plate at 70% confluency and co-transfected with the appropriate pHR expression plasmid and lentiviral packaging plasmids (pMD2.G and p8.91 – gifts from the Trono lab) using Fugene HD transfection reagent. Viral supernatants were collected 2 days after transfection and passed through a 0.45 mm filter.

NIH 3T3 cells to be infected with lentivirus were plated in a 6 well dish at 20%–40% confluency. After adherence to the plate, 10-100 μL of filtered virus were added to the cells. 24 hr post-infection, viral media was replaced with normal growth media and cells were imaged at least 48 hr after infection to allow time for integration and expression.

Generation of clonal chassis cell line

First, wild-type NIH 3T3 cells were co-transfected with a plasmid bearing the Super PiggyBac transposase and a second plasmid, pUC piggyBac, containing the optogenetic system components- *phyB*, *bfp-erk*, *iRFP-PIF-SOScat* – as well as a puromycin resistance gene for selection and construct maintenance. Fragments encoding key domains were amplified from plasmids using PCR and ligated into pHR lentiviral backbones, PiggyBAC transposase vectors, or CRISPR-compatible vectors using Gibson assembly (New England Biolabs, Ipswitch MA).

After undergoing one week of selection in puromycin these cells were sorted once for high *bfp-erk* expression. Following the transposed cell population was then infected with lentivirus bearing the *mcp-mCherry* and *h2b-diRFP* genes. This twice-modified population was then sorted for single-cell clones using fluorescence activated cell sorting (FACS) gating for single cells that expressed both high levels of *bfp* expression as well as intermediate levels of *mCherry* expression- with each gated channel representing one of the two separate genomic integration events. Clones were grown in cell culture treated 96 well plates in a 1:1 ratio of DMEM + 10% FBS and NIH 3T3 conditioned media. After 2 weeks clones were evaluated for light-dependent translocation of iRFP-PIF to the membrane as well as light-dependent nuclear translocation of BFP-Erk. Upon passing both of these tests cells were expanded, aliquoted, and frozen down in liquid nitrogen for future experimentation and CRISPR tag integration.

CRISPR integration and isolation of native loci tagged IEGs

For each IEG to be tagged a plasmid was constructed with 2 kb of upstream genomic homology and downstream genomic homology, as predicted by the mm9 mouse genome assembly, flanking, in-frame, the codons for msfYFP followed by a stop codon and 24x repeats of the MS2 RNA aptamer. DNA strands with genomic homology were isolated using PCR, using PrimeSTAR GXL polymerase from Clonetech, with genomic DNA templates isolated by Epicenter QuickExtract DNA extraction solution following the manufacturers' guidelines. Plasmids were transformed into One Shot Stbl3 chemically competent *E. coli* to avoid loss through recombination of the MS2 repeats. Genomic targeting was done using the pX330 plasmid expressing Cas9 nuclease as well as a unique gRNA for each tagged IEG. gRNAs were inserted into this plasmid using BbsI digestion as has been previously reported (Xue et al., 2014). Candidate gRNAs were first selected for proximity to the stop-codon of the candidate IEG. Only gRNAs that would result in a double-stranded cut > 30 bp away from the stop codon were considered. Next gRNAs were filtered for their off-target activity using the Zhang Lab's gRNA design tool (http://crispr.mit.edu/). Finally gRNAs were eliminated if, upon cutting and directing homologous recombination of the msfYFP-MS2 tag, the entire gRNA-binding, genomic site remained intact. For gRNAs that did not already begin with a guanine nucleotide one was added. Single-stranded gRNAs with 20 bp overhangs were synthesized by Integrated DNA Technologies, annealed, and inserted into BbsI-digested pX330 plasmid using Gibson assembly. All plasmids were verified by restriction enzyme digest followed by insert sequencing.

The chassis cell-line or other NIH 3T3 derived line was plated to a low to intermediate confluency (20%–40%) in six-well dishes and 2.5 μg of both purified plasmids, pX330 and homology bearing, were co-transfected using Lipofectamine LTX & Plus reagent by Life Technologies using Opti-MEM as the vehicle according to the manufacturer's guidelines. Media was replaced with fresh DMEM + 10% FBS after 24 hr. Cells were checked for msfYFP fluorescence by confocal fluorescence microscopy 3 days after transfection and then bulk-sorted for msfYFP expression using FACs.

Cell preparation prior to imaging

For all imaging experiments cells were plated on 96-well, black-walled, 0.17 mm high performance glass bottom plates from In Vitro Scientific that had been pretreated with 10 μg/ml fibronectin in phosphate buffer saline (PBS). Cells were allowed to adhere overnight in DMEM + 10% FBS. To activate the Phy-PIF optogenetic system 10 μM phycocyanobillin in DMSO was added to cultures for 1 hr. Cells were maintained under continuous 750 nm deactivating light supplied by custom designed LED-bearing circuit boards. Four hours prior to the experiment DMEM + 10% FBS was exchanged by washing cells twice in DMEM + 1 mg/ml Bovine Serum Albumin (BSA). Media exchanges were done in the dark using Energizer Vision HD headlamps modified with 750 nm LEDs. Just prior to imaging 50 μL of mineral oil was added to the top of each well to stop evaporation.

Imaging

Cells were maintained at 37°C with 5% CO2 for the duration of an imaging experiment. Confocal microscopy was performed on a Nikon Eclipse Ti microscope with a Prior linear motorized stage, a Yokogawa CSU-X1 spinning disk, an Agilent laser line module containing 405, 488, 561 and 650 nm lasers, and an iXon DU897 EMCCD camera.

Optogenetic stimulation hardware

For microscopy experiments both 650 nm red and 750 nm infrared light was delivered using two X-Cite XLED1 light sources. XLED1s were individually coupled to their own Polygon400 Mightex Systems digital micromirror device to control the temporal dynamics of light inputs. For all other experiments light inputs were delivered through custom 36-LED printed circuit boards with all LEDs wired to a single power source.

Quantification of transcriptional foci

Transcriptional bursts were quantified using a semi-automated procedure. First bursting cells were imaged by taking a 7-layered z stack spanning 4 μm (0.8 μm between z-slices), which was centered on the medial Z-plan of the nuclei of interest. The maximum projection in the Z dimension was then computed to bring all imaged bursts into the same plane. Positional information about the location of each burst over time was then annotated by hand using the ImageJ 'measure' tool. Hand tracking was necessary to exclude the quantification of burst-like debris floating in the imaging field that could be confused as bursts. From there we developed a MATLAB script that (a) identifies a burst region in the maximum intensity projected time series, (b) fits a 2-dimensional Gaussian to the identified region whose parameters were limited to exclude relatively large underlying fluctuations in background intensity, and (c) calculates the integrated area under the fit Gaussian as the burst intensity.

Drug treatment

All drug additions were done using 200 μL gel-loading tips. Drugs were pre-diluted to a 1:10 stock concentration in the current experimental media and added directly to cells on the microscope. Final drug concentrations were: Cycloheximide 100 μg/ml, Actinomycin D 100 μg/ml, PDGF 10 ng/ml and Doxorubicin 1 μM.

Immunofluorescence staining

Cells were first fixed with Cytofix from BD Biosciences according to manufacturers instructions and then permeablized with 100% ice-cold methanol. Samples were re-suspended in immunofluorescence buffer (PBS, 10% FBS, 2 mM EDTA) and blocked for 1 hr at room temperature. For staining phosphorylated Erk samples were incubated with anti-phospho-p44/42 MAPK (Erk1/2) (Thr202/Tyr204) rabbit mAb (Cell Signaling) #4370 was diluted 1:200 in immunofluorescence buffer at 4°C overnight. Cells were then washed 5 times in immunofluorescence buffer + 0.3% (V/V) Triton 100-X (IF-Triton) and incubated with anti-rabbit secondary for 1 hr at room temperature. Finally cells were washed 5 times with IF-Triton and imaged in the presence of 1 μg/ml DAPI.

CELL LYSATE COLLECTION/WESTERN BLOTS

Media was aspirated from cells grown in 6-well (9 cm^2) tissue culture treated dishes. Cells were immediately lysed in 120 μL ice-cold RPPA lysis buffer (1% Triton X-100, 50mM HEPES, pH 7.4, 150mM NaCl, 1.5mM MgCl2, 1mM EGTA, 100mM NaF, 10mM Na pyrophosphate, 1mM Na3VO4, 10% glycerol, freshly added protease and phosphatase inhibitors from Sigma-Aldrich Cat# 11836170001 and 04906837001, respectively). Cell lysates were collected in microfuge tubes and centrifuged at 13,000 rpm for 10 min at 4°C. Supernatants were collected and then mixed with 4x NuPAGE LDS sample buffer and heated at 95°C for 5 min. Samples were then loaded onto 4%–12% Bis-Tris gels, transferred to nitrocellulose, probed with primary and secondary antibodies and imaged using a Li-Cor Odyssey CLx imaging system.

Mathematical model of Erk-to-transcription dynamic transmission

State variables

E: Erk protein
m: *dusp* mRNA
p: DUSP protein
m_i: target mRNA

Inputs

$u(t)$: pathway input (OptoSOS induced Ras activity), which we choose to take the values {0, 10} depending on whether light is OFF or ON, respectively.

It has been experimentally observed that ppErk pulses occur with a similar pulse width but variable time between pulses (Albeck et al., 2013; Hiratsuka et al., 2015). Pulses in Erk activity can occur as frequently as once per 20 min (Shankaran et al., 2009) or as rarely as one per 4 hr (Aoki et al., 2013). We thus simulated Erk pulses on this experimentally measured timescale (e.g., 20 min pulses of input, repeating every 20 min to multiple hours).

Model equations

Our model comprises 4 equations:

$$\frac{dE}{dt} = u(t) - \gamma E - \delta p E$$

$$\frac{dm}{dt} = \frac{E^n}{K_1^n + E^n} - \gamma m$$

$$\frac{dp}{dt} = m - \gamma p$$

$$\frac{dx_i}{dt} = \frac{E^n}{K_{2i}^n + E^n} - \gamma_i x$$

Parameters

There are four basic parameters in our model. Two parameters (K_1 and δ) characterize our negative feedback loop, one representing the strength of Erk-induced DUSP transcription and the other representing the DUSP-induced dephosphorylation of Erk. One degradation rate (γ) characterizes the basic transition rates of Erk activation, mRNA production and protein accumulation. For simplicity these three transitions through the central dogma are assumed to occur on a similar timescale. This assumption is accurate within an order of magnitude, as we have measured the delays experimentally in (Toettcher et al., 2013) and Figures 3D–3E to be 10-30 min. Finally, we assume some cooperativity in the ability of nuclear ppErk to induce gene expression, and between DUSP expression and nuclear ppErk inhibition.

For all simulations in Figure 5, the parameter values were chosen are as follows:

$$K_1 = 0.05$$
$$\delta = 50$$
$$\gamma = 1$$
$$n = 2$$

There are also two parameters per target gene that represent their activation by nuclear ppErk, and their degradation rate:

$$K_i = \text{variable}$$
$$\gamma_i = \text{variable}$$

These do not affect Erk or DUSP dynamics (which are completely specified by inputs and the negative feedback loop above) but rather reflect potential gene-to-gene variations Erk sensitivity (K_i) or rate of turnoff in the absence of input (γ_i).

Simulating the model

Model simulations were conducted in Python 3 using the Anaconda 4.3 distribution from Continuum Analytics. Numerical simulations were conducted using the odeint function from the SciPy v0.18.1 scipy.integrate module, which is used as a wrapper for the USCD1227 LSODA ordinary differential equation solver for stiff or non-stiff systems.

All computational experiments can be found in the Supplementary iPython notebook (Data S1). After defining the nonhomogeneous, pulse-delivering, input function $u(t)$ we defined a function, nfDeg, capturing our description of the model. Initial conditions, state0, were set to 0 and a typical pulse input sequence was simulated for 350 min (modeled time) with 20 min input pulses separated by 60 min off periods. All state variables were then plotted using the matplotlib plotting library.

For band-pass input scan experiments the simulation time was increased to 10,000 min to avoid artifacts resulting from the averaging system outputs with different period lengths. This substantially increased simulation time and memory. The first 2 input periods for each stimulation were omitted from calculations of the average output to avoid the 'first burst effects' and better represent the model behavior as $t \rightarrow \infty$. For these computations the parameter corresponding to promoter affinity, K_{2i}, was varied over two orders of magnitude, from 0.1 to 10.

For simulations where the negative feedback was removed the rate of creation of negative feedback protein Dusp was simply multiplied by 0. Band-pass experiments for these systems were run the same as those with negative feedback.

For degradation rate scans the parameter γ_i was varied by five orders of magnitude, from 0.01 to 100.

QUANTIFICATION AND STATISTICAL ANALYSIS

All quantification was performed using ImageJ or MATLAB and statistical analysis was performed using MATLAB. Data are typically presented as mean ± SEM as specified in the figure legends.

DATA AND SOFTWARE AVAILABILITY

The accession number for the raw and analyzed RNA-seq data reported in this paper is GEO: GSE100816.